

## A MODIFIED STRATIFIED MODEL FOR 3C 273 JET

Wen-Po Liu<sup>1,2</sup> and Zhi-Qiang Shen<sup>1</sup>

<sup>1</sup> Shanghai Astronomical Observatory, Shanghai 200030, P.R.China; [wpliu@shao.ac.cn](mailto:wpliu@shao.ac.cn);  
[zshen@shao.ac.cn](mailto:zshen@shao.ac.cn)

<sup>2</sup> The Graduate School of Chinese Academy of Sciences, Beijing 100049, P.R.China

**Abstract** We present a modified stratified jet model to interpret the observed spectral energy distributions of knots in 3C 273 jet. Based on the hypothesis of the single index of the particle energy spectrum at injection and identical emission processes among all the knots, the observed difference of spectral shape among different 3C273 knots can be understood as a manifestation of deviation of the equivalent Doppler factor of stratified emission regions in individual knot from a characteristic one. The summed spectral energy distribution of all the ten knots in 3C 273 jet can be well fitted by two components, low-energy (radio to optical) component dominated by the synchrotron radiation and high-energy component (UV, X-ray and  $\gamma$ -ray) dominated by the inverse Compton scattering of the cosmic microwave background. This gives a consistent spectral index of  $\alpha = 0.88$  ( $S_\nu \propto \nu^{-\alpha}$ ) and a characteristic Doppler factor of 7.4. Assuming the average of the summed spectrum as the characteristic spectrum of each knot in the 3C273 jet, we further get a distribution of Doppler factor. We discuss the possible implications of these results for the physical properties in 3C 273 jet. Future GeV observations with *GLAST* could separate the  $\gamma$ -ray emission of 3C 273 from the large scale jet and the small scale jet (i.e. the core) through measuring the GeV spectrum.

**Key words:** galaxies: active — galaxies: individual (3C273) — galaxies: jets — radiation mechanisms: non-thermal

### 1 INTRODUCTION

Being nearby ( $z=0.158$ ), the jet of 3C 273 which was the first quasar discovered (Schmidt 1963) has been studied extensively from the radio (e.g., Conway et al. 1993), infrared (e.g., Jester et al. 2005; Uchiyama et al. 2006, hereafter U06; Jester et al. 2007, hereafter J07; Wen et al. 2002), optical (e.g., Jester et al. 2001; 2005; Lin 2006; Qian 2001), to the X-rays (e.g., Marshall et al. 2001; Sambruna et al. 2001, hereafter S01; Jester et al. 2006, hereafter J06). Chaotic feature in the light curve of 3C 273 is also discussed by Liu (2006). A TeV flux upper limit has also been obtained by shallow *High Energy Stereoscopic System* (H.E.S.S.) observations (Aharonian et al. 2005). The 10''-long radio jet has a knotty morphology, with the first bright knot at about 12''-13'' from the central engine and increasing radio intensity toward a terminal bright hot spot about 22''-23'' from the nucleus (Flatters & Conway 1985; U06).

Based on the spectral energy distributions (SEDs) of these knots and hot spots in 3C 273 jet, many researchers have identified two-component nature (U06; J06; S01), namely (1) the low-energy component extending from radio to optical, and (2) the high-energy component responsible for the emission including X-ray. Synchrotron emission is considered to be the dominant radiation mechanism from radio through optical bands, i.e., the low-energy component (S01; U06), but the radiation mechanism of X-ray emission is still perplexing. So far, there have been three candidates for the origin of the X-rays (S01): (a) synchrotron emission which another much more energetic population of particles emit (Röser et al. 2000; Aharonian 2002; Bai & Lee 2003; U06); (b) inverse Compton scattering of synchrotron photons from low energy component, i.e. Self-Synchrotron Compton (SSC) model; and (c) inverse Compton scattering of photons

which are external to the jet such as inverse Compton scattering of cosmic microwave background photons model (hereafter IC/CMB).

SSC emission from electrons in an equipartition magnetic field can usually account for the X-ray emission from hot spots (J07, Harris & Krawczynski 2006). But S01 and J06 showed that the contribution from SSC X-rays in 3C 273 jet is not significant, so we provisionally ignore SSC effect on the X-ray emission. Georganopoulos et al. 2006 (hereafter G06) have presented some diagnostics (the synchrotron model needs multi-TeV electrons responsible for production of the X-rays, but the IC/CMB model requires a cutoff which is lower than TeV in the SED) to distinguish the synchrotron and IC/CMB models. And the  $\gamma$ -ray predicted by these two models, can be tested through GeV and TeV observations of the 3C 273 large-scale jet. U06 described the wide radio-to-X-ray spectrum with their double power-law models (Eq. (1) of U06, low-energy component with an exponential cutoff), but they required an additional assumption that the two power-law indices were different and their formula was partly man-made rather than derived from any clear physical insight. The double synchrotron emission model also does not clearly point out the direct connection of the two populations of source particles, and the second, the ultra-energetic particles that emit X-ray photons calls for a radical rethink of the physics of relativistic jet that black holes drive (Urly 2006).

Among the suggested mechanisms for the high-energy component, we adopt IC/CMB model if there is a bulk relativistic motion on kiloparsec scales (S01). Indeed, VLBI observations have detected apparent superluminal motions in the parsec-scale jet with apparent velocities  $\sim 6$ -10  $c$  (e.g., Unwin et al. 1985). And X-ray/optical emission remains asymmetric, implying the presence of relativistic bulk motion on kiloparsec scales (S01) too. J06 presented deeper Chandra observations of 3C 273 jet and found that the X-ray spectra are softer than the radio spectra in nearly all parts of the jet, ruling out the simplest one-zone beamed IC/CMB models for the X-ray emission from the entire jet. Within their two-zone jet model, they still required two different spectral indices for radio and X-ray spectrum of each knot in 3C 273 jet. G06 sum the fluxes of 3C 273 knots excluding the bright knots A and B as a “big knot”, and they have predicted the  $\gamma$ -ray emission of the 3C 273 large-scale jet by applying (not fitting) IC/CMB model to the “big knot”. S01 divided all the detected knots into four regions, and then quite well fit IC/CMB model to the wide-band SED in each of them, implying the rationality of IC/CMB model for 3C273 jet. Then the question is why IC/CMB model could fit the regions enclosing some neighboring knots but not individual knot. S01, J06 and G06 did not explain this interesting problem. This problem may be related to the small viewing angles of knots with the stratified structure (see § 2). As a result, the observed spectral shape may be modulated by different beaming effects on the flux. S01’s enclosing some neighboring knots thus minimizes the deviation of spectrum from that of a single component.

By now, all the fitted models on the SEDs of knots in 3C 273 jet have assumed a single Doppler factor for emission regions in the 3C273 knots and different spectral indices for the inner and outer knots (U06; J06; S01). Based on the analysis of Liu & Shen (2007) (hereafter LS07) on the radiation mechanism of knots in the M87 jet, the fitted energy spectral indices of the source particles along the jet were nearly constant, suggesting the identical acceleration and radiation mechanism for the source particles along the jet. We would try a different way (partly similar to S01 and G06’s management of enclosing some neighboring knots) to investigate what resulted in the observed SEDs of knots in 3C 273 jet.

In § 2, we describe in detail our model and management for SEDs of knots in 3C 273 jet. In § 3, we present and discuss the fitting results of this model to the summed SED of all the knots in 3C 273 jet and give the distribution of the Doppler factor in the emission regions among all the knots. A summary is given in § 4.

## 2 A MODIFIED STRATIFIED JET MODEL AND MANAGEMENT FOR THE SPECTRA OF KNOTS

The effect of the stratified emission along the jet and the effect of different emitting regions through the jet’s cross section are common for the observed knot emission (Perlman et al. 1999, Marshall et al. 2002, Perlman & wilson 2005, Harris & Krawczynski 2006). Based on the difference between the optical and radio polarimetric observations, Perlman et al. (1999) advanced a model of partial energy stratification. They illustrated that the optical-emitting electrons are located closer to the jet axis, while most of the radio-emitting electrons are located nearer the jet surface. Further promoting this model, we think that even the

optical- and radio-emitting electrons themselves may also be stratified through the jet's cross section, similar to the spine-sheath structure.

And the advection and diffusion of the populations of particles along the jet with the decrease of the synchrotron lifetime from low energy to high energy would result in spatially stratified (LS07) and conical emission layers (regions) along the jet. Because of cooling process, the stratified effect along the jet may be more obvious for high energy electrons. This scenario suggests that the observed different radiation from a knot at different frequency is not from a simple electrons component within the same region of that knot, but from a more complicated one whose stratified emission layers roughly correspond to different synchrotron-emitting electrons (and so to different emissions). This is more significant for a jet with small viewing angle. If the stratified emission layers were almost independent on each other (i.e., different emission regions could have different intrinsic velocities and/or electrons distribution), their Doppler factors may be different. Otherwise the Doppler factors should be similar to each other. If we further assume that all the conical emission layers had a same intrinsic velocity but electron distribution of each emission layer was asymmetrical to the jet axis, this results in that the equivalent/averaged viewing angle of each emission layer could have two phases, i.e., near and away from line of sight.

The model considered here is basically composed of two components with synchrotron radiation dominating the low-energy band and the IC/CMB dominating the high-energy emission. We adopted the synchrotron model of LS07 to describe the low-energy component. In the model (Eq. (3) of LS07), they considered a decay of spectral index of injection particles possibly due to the sum of the injection spectrum from different acceleration sources with synchrotron losses in the thin acceleration region, so there are two break frequencies (Eq. (5) in LS07) at two sides of which the spectral index changes for the spectra of knots in AGN jet. The IC/CMB spectrum is an identical copy of the synchrotron one. But since 3C 273 jet in high-energy component was only detected from UV to X-ray, we use the power law distribution to describe the spectrum below the first break frequency which falls in  $\gamma$ -ray band.

Our modified stratified jet model showed that the stratified emission layers in a knot may have different equivalent/averaged Doppler factors (i.e., Doppler factors may be roughly a function of synchrotron frequency). Especially, when the bulk velocity of advection in 3C 273 jet approaches to the light speed and the equivalent/averaged viewing angle of emission layers is very small, both the Doppler factor and apparent motion of emission regions in the 3C273 knot are sensitive to the change of velocities and equivalent viewing angles of emission layers. For synchrotron emission, the observed fluxes ( $S_\nu \propto \nu^{-\alpha}$ ,  $\alpha$  is spectral index) at different frequencies are related to their Doppler factors by  $S_{\nu_1}/S_{\nu_2} = (\delta_1/\delta_2)^{3+\alpha} \times (\nu_1/\nu_2)^{-\alpha}$  (Dermer 1995), and for IC/CMB emission, the relation is  $S_{\nu_1}/S_{\nu_2} = (\delta_1/\delta_2)^{4+2\alpha} \times (\nu_1/\nu_2)^{-\alpha}$  (Dermer 1995). This flux ratio is very sensitive to the ratio of the Doppler factors, implying that different bulk velocities and the equivalent viewing angles (i.e., different equivalent Doppler factors) can easily cause the difference in the spectral shape of knots in 3C 273 jet.

Because we do not know the real Doppler factor distribution for emission regions along 3C 273 jet, in our analysis we assumed that the deviations of observed spectral shape for emission regions along 3C 273 jet is somehow symmetric to a hypothetic characteristic one and then we obtain such a characteristic one by averaging SEDs of all the knots in 3C 273 jet. This is justified by the reasonable fitting results of the spectral shapes and Doppler factors (see § 3). As such, the increasing lower-energy emissions and decreasing high-energy emissions with the increasing separation from the nucleus (U06) can be ascribed to the deviation of Doppler factor of each knot from the characteristic one in 3C 273 jet. The detailed distribution of magnetic field and electron velocity directions may also affect the observed spectral shape of knots, but for simplicity, we do not consider this case. The SED of individual knot in the M87 Jet (with a larger viewing angle than 3C273 Jet) could be fitted by a continuous injection (CI) synchrotron with a break power law (LS07), but this is not the case in 3C273. By assuming the effects of intrinsic conditions (such as volume, kinetic age, electron normalization constant and distribution of magnetic field and electron velocity directions etc.) of jets in M87 and 3C273 are similar on the observed synchrotron spectrum of individual knot, we think that the deviation of the observed spectral shape of individual knot in 3C 273 jet from the CI synchrotron one is caused by some external effects likely being related to the different viewing angles. According to this viewpoint, the spectrum of every knot in 3C 273 jet is modulated by different equivalent Doppler factors in the stratified emission layers, resulting in the models with a single Doppler factor to be ineffective for knots (such as IC/CMB in J06). But the summed spectrum of all the knots may minimize such an effect

(partly similar to S01' management of enclosing some neighboring knots) and therefore can be treated as a representative SED of a "big knot" with a single Doppler factor and spectral index. In the following, unlike G06's illustration (not fitting) of a "big knot" (excluding the bright knots A and B), we will first get a quantitative description of the characteristic spectrum of our "big knot" (including all the 3C 273 knots) by means of two-component fitting. Then, we will discuss the deviation of Doppler factors in each knot by comparing their SEDs with this characteristic one.

### 3 FITTING RESULTS AND DISCUSSION

In Table 1, the data of knots except knot H1 were from J07. For knot H1, the *VLA* and *HST* data are from Jester et al. (2005), and the *Spitzer* data from U06. It was not detected by *Chandra* at X-ray and other three *HST* bands. The error bars for the radio, optical and X-ray data were separately estimated by increasing 5-20 times the r.m.s noise in J07, within the range of the flux errors (1%-5% in all cases for both the radio and optical measurements, less than 10% for most of the X-ray measurements, U06). A formal fractional uncertainty of 10% is assigned to the *Spitzer* data to account for systematic errors of 2%-10% (U06). By adding up the flux densities and error bars of all the knots in 3C 273 jet, we obtained the SED for the  $10''$ -long jet (as a "big knot"). We then performed the weighted least-squares method to fit the two-component model to this SED.

Before fitting, we need to divide the available 10 data points from radio to X-rays into two groups to match the corresponding low- and high-energy components. By examining the shape of the SED in Fig. 1, it is likely that the cutting frequency between the two components is around  $1.0 \times 10^{15}$  Hz. This makes it difficult to decide the dominant mechanism for the *HST* measurement at  $1.0 \times 10^{15}$  Hz. Therefore, we first did two fits of the low-energy synchrotron emission to the data sets with and without  $1.0 \times 10^{15}$  Hz measurement, respectively. We found that the fitting with this *HST* data point gave a 3-4 times larger reduced chi-squares ( $\chi_\nu^2$ ). Thus, we chose to interpret the emission at  $1.0 \times 10^{15}$  Hz being dominated by the IC/CMB. So, the cutoff frequency between the upper limit frequency of the low-energy component and the lower limit frequency of the high-energy component is within  $4.85 \times 10^{14}$  to  $1.00 \times 10^{15}$  Hz.

Once we fixed such a cutoff frequency, we can perform independent spectral fitting to both low- and high-energy components as described in § 2. In practice, we fit the synchrotron model (Eq. (5) of LS07, with 4 parameters) to the 7 data points at frequency lower than  $1.0 \times 10^{15}$  Hz. In this process, a power-law form is chosen near the break frequencies because we only need to be concerned with the trend of the break frequencies. There are two break frequencies in our model, but we do not know exactly where they are when we fit to the chosen data in Fig. 1. So we first arbitrarily divide observational data into three groups to perform the fitting and calculate the corresponding  $\chi_\nu^2$  by changing the division. All the possible combinations are tried before we obtain the best fit with a minimal  $\chi_\nu^2$  among them. For the high-energy component fit to the remaining 3 high frequency data points, only a power law (with 2 parameters) is needed. In Table 2 are shown the fitting results. The SED for the "big knot" in 3C 273 jet and the best fits are plotted in Fig. 1. Therefore, both the high and low-energy components are independently described by our model. The fitted spectral indices of the low-energy ( $0.87 \pm 0.02$ ) and high-energy ( $0.88 \pm 0.02$ ) components are well consistent with each other, supporting the IC/CMB nature of the high-energy component. The corresponding value of the particle spectral index ( $p = 2\alpha + 1$ ) of 2.76 is also among the characteristic range ( $2 < p < 3.5$ , Blumenthal & Gould 1970).

The fitted synchrotron component has a total power of  $L_s \approx 5.2 \times 10^{41}$  erg s $^{-1}$ , which is actually dominated by the emission around the peak frequency, i.e.,  $L_s \approx 4\pi D_L^2 [\nu_{s,p} S(\nu_{s,p}) / (1 - \alpha) + \nu_{c,p} S(\nu_{c,p}) / (\alpha - 0.5)]$ , here  $S(\nu_{s,p})$  is the flux density at the peak frequency  $\nu_{s,p} \approx 1.10 \times 10^{13}$  Hz (see Table 2), and a luminosity distance of  $D_L = 749$  Mpc is adopted. Accordingly, we can estimate the luminosity of IC/CMB emission, which is also dominated by the emission around its peak frequency  $\nu_{c,p}$ . Thus, we can get a ratio between IC/CMB luminosity and synchrotron luminosity as follows

$$\frac{L_c}{L_s} = \frac{\nu_{c,p} S(\nu_{c,p})}{\nu_{s,p} S(\nu_{s,p})}. \quad (1)$$

According to Geoganopoulos et al. (2006), this luminosity ratio is related to the Doppler factor as

$$\frac{L_c}{L_s} = 6.25 \times 10^{-4} \delta^4, \quad (2)$$

**Table 1** Flux Densities of Knots in 3C 273 jet. <sup>1</sup>The data of the knots except knot H1 were from J07. The *VLA* and *HST* data of knot H1 were from Jester et al. (2005), but the *Spitzer* data of knot H1 were from U06. <sup>2</sup>The error bars for the *VLA*, *HST* (except for  $1.86 \times 10^{15}$  Hz) and *Chandra* data were separately estimated by increasing 5-20 times of r.m.s noise in these data from J07. <sup>3</sup>A formal fractional uncertainty of 10% is assigned to the *Spitzer* data to account for the systematic errors of 2%-10% (U06). <sup>4</sup>The sum of the flux densities and error bars for the knots in the 3C273 jet.

Frequency (Hz)	Flux Density <sup>1</sup>										Sum <sup>4</sup>	
	A	B1	B2	B3	C1	C2	D1	D2H3	H2	H1		
<i>VLA</i> <sup>2</sup> (mJy):												
$8.33 \times 10^9$	90.5 ± 1.30	69.2 ± 1.07	105 ± 1.43	50.8 ± 1.01	101 ± 1.56	205 ± 2.47	283 ± 3.9	836 ± 8.84	1330 ± 16.90	571.9 ± 7.27	3400.5 ± 45.75	
$1.5 \times 10^{10}$	58.9 ± 0.66	41.9 ± 0.53	69 ± 0.77	34.8 ± 0.59	67 ± 0.90	134 ± 1.56	182 ± 2.34	516 ± 5.33	782 ± 9.62	398.4 ± 4.90	2085.6 ± 27.20	
$2.25 \times 10^{10}$	38.5 ± 0.49	30.6 ± 0.42	50.8 ± 0.60	23.6 ± 0.43	48.8 ± 0.69	97.1 ± 1.12	131 ± 1.69	357 ± 3.64	520 ± 6.24	208.0 ± 2.50	1427.4 ± 17.82	
<i>Spitzer</i> (μJy):												
$5.23 \times 10^{13}$	45 ± 10	35 ± 12	36.2 ± 8.1	12.8 ± 2.9	98 ± 11	89 ± 12	154 ± 15.4 <sup>3</sup>	161 ± 16.1 <sup>3</sup>	87 ± 12	28 ± 11	746 ± 110.5	
$8.45 \times 10^{13}$	27 ± 2.7 <sup>2</sup>	15 ± 2.6	28.8 ± 2.88 <sup>3</sup>	10.2 ± 1.02 <sup>3</sup>	36 ± 3.6 <sup>3</sup>	46 ± 4.6 <sup>3</sup>	80 ± 8 <sup>3</sup>	140 ± 14 <sup>3</sup>	41 ± 4.1 <sup>3</sup>	10 ± 2.6	434 ± 46.1	
<i>HST</i> <sup>2</sup> (μJy):												
$1.87 \times 10^{14}$	11.3 ± 0.48	4.9 ± 0.17	10.2 ± 0.20	4.84 ± 0.12	10.8 ± 0.17	18.1 ± 0.20	21.7 ± 0.19	40 ± 0.28	6.97 ± 0.19	2.04 ± 0.06	130.31 ± 2.06	
$4.85 \times 10^{14}$	4.93 ± 0.12	1.83 ± 0.082	3.86 ± 0.098	1.37 ± 0.059	2.93 ± 0.079	3.93 ± 0.09	3.56 ± 0.08	7.68 ± 0.1	1.29 ± 0.09	...	31.38 ± 0.72	
$1.00 \times 10^{15}$	3.2 ± 0.17	0.973 ± 0.06	1.88 ± 0.07	0.507 ± 0.04	1.16 ± 0.06	1.28 ± 0.06	1.09 ± 0.05	2.54 ± 0.07	0.459 ± 0.07	...	13.09 ± 0.65	
$1.86 \times 10^{15}$	2.03 ± 0.11	0.626 ± 0.037	1.47 ± 0.079	0.439 ± 0.028	0.657 ± 0.039	0.723 ± 0.042	0.679 ± 0.04	1.39 ± 0.075	0.288 ± 0.02	...	8.302 ± 0.47	
<i>Chandra</i> <sup>2</sup> (nJy):												
$2.42 \times 10^{17}$	46.5 ± 2.70	10.9 ± 1.25	20 ± 1.65	3.41 ± 0.70	4.85 ± 0.80	6.25 ± 0.90	5.16 ± 0.85	7.82 ± 1.00	1.3 ± 0.45	...	106.19 ± 10.30	

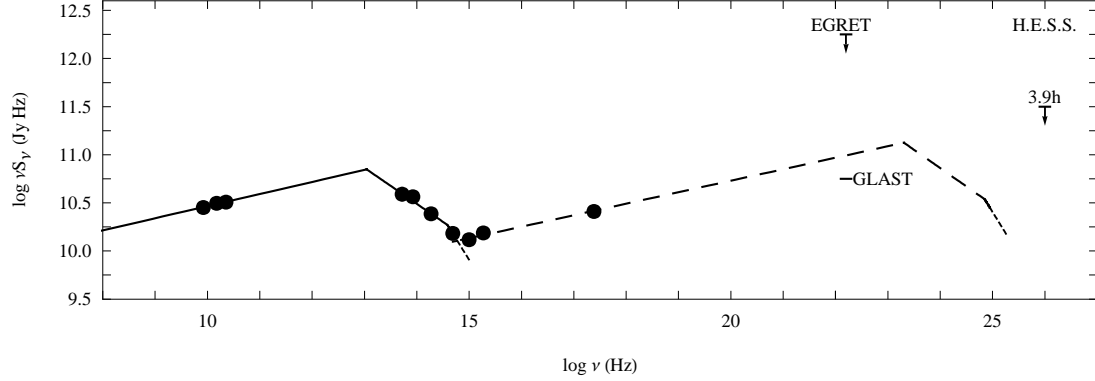


**Fig. 1** The SED for the summed knots in 3C 273 jet from radio through X-ray wavelengths. The solid line displays model fit to the low-energy component, and the dashed line to the high-energy component. The dotted lines show the possible cutoff frequency band for the two components. The error bars of most measurements are too small to be seen here. The EGRET upper limit and the *GLAST* sensitivity limit are also shown, as well as a TeV flux upper limit from shallow H.E.S.S. observations (Aharonian et al. 2005).

**Table 2** Parameters of Model Fits to Radio through X-ray Data. Col. (1): Component designation. Col. (2): Model designation. Col. (3): Spectral index. Col. (4): Reduced chi square. Col. (5): Peak frequency, note that the peak frequency for high-energy component is a derived parameter. Col. (6): Characteristic Doppler factor.

Parameters	Model	$\alpha$	$\chi^2_\nu$	$\nu_{peak}(\text{Hz})$	$\delta$
Low-energy Component	Synchrotron	$0.87 \pm 0.02$	1.18	$1.10 \times 10^{13}$	$7.4 \pm 0.5$
High-energy Component	IC/CMB	$0.88 \pm 0.02$	1.51	$2.00 \times 10^{23}$	...

and the two peak frequencies ( $\nu_{c,p}$  and  $\nu_{s,p}$ ) are related by the expression

$$\nu_{c,p} = 3.3 \times 10^8 \delta^2 \nu_{s,p}. \quad (3)$$

It should be mentioned that in getting Eqs. (2) and (3), an equipartition magnetic field  $B\delta \approx 2 \times 10^{-4}\text{G}$  (Jester et al. 2005) is used. These equations require that the electrons which emit synchrotron photons (i.e., the first component of the SED) upscatter the CMB and, the resulting IC/CMB SED (i.e., the second component) is an exact copy of the synchrotron one (G06). This is consistent with our model for the large scale jet as a “big knot” (our synchrotron model is somewhat different from the one of G06, but this doesn’t influence the validity of the equations in the letter), so these equations are still valid in our model. Finally, from our fitting results, we can obtain the characteristic Doppler factor  $\delta \approx 7.4$  which well agrees with the requirement of FSRQ’s Doppler factor ( $> 6.45$ , Cao & Bai 2008). This may verify the Uniform Scheme of quasars (Urry & Padovani 1995). The frequency shift of IC/CMB and synchrotron emissions ( $\nu_c \sim 1.81 \times 10^{10}\nu_s$ ), here  $\nu_c$  and  $\nu_s$  are the observed IC/CMB and synchrotron frequencies, respectively. Then we could estimate the equipartition magnetic field  $B = 27\mu\text{G}$  and a synchrotron lifetime of  $\sim 4000\text{yr}$ , (Eq. (4) of U06) of the “big knot” which is smaller than the source kinetic age ( $10^5 \sim 10^7\text{yr}$ , U06), this means a continuous injection of electrons responsible for the SED of the 3C273 jet. The peak frequency of the high-energy component is at  $2.00 \times 10^{23}\text{ Hz} \sim 1\text{ GeV}$  (see Table 2), around the working band of the *Energetic Gamma-Ray Experiment Telescope* (EGRET) on the *Compton Gamma-Ray Observatory* (CGRO) and the current *Gamma-Ray Large Area Space Telescope* (*GLAST*). The model predicted  $\gamma$ -ray flux was at least 10 times lower than the EGRET upper limit (Sreekumar et al. 1994; Geoganopoulos et al. 2006), but

should be detectable by the *GLAST* (see Fig. 1). Although the *GLAST* (e.g., the expected 68% containment angular resolution of *GLAST* LAT is  $0.15^\circ$  (on-axis) for photons above 10 GeV, *GLAST* website) could not separate the  $\gamma$ -ray emission from the large scale jet and the core, by measuring the SED of the GeV energies, we still could identify the origin of the GeV emission (the large scale jet or the small scale jet, i.e. the core). The high-frequency cutoff of the second component appears at the band between  $8.8 \times 10^{24}$  and  $1.8 \times 10^{25}$  Hz (lower than TeV band), which is consistent with the non-detection by shallow *H.E.S.S.* observations (Aharonian et al. 2005) as shown in Fig. 1.

Based on the model described in § 2., the observed spectrum of individual knot in 3C 273 jet may result from the stratified emission layers in which the Doppler factors deviate from the characteristic one. So, unless removing the deviation effect of Doppler factors in the observed spectrum of each knot, those fitted spectral indices for radio and X-ray bands of each knot (Jester et al. 2005; J06; J07) didn't really reflect the intrinsic and characteristic spectral shape of 3C273 jet. Here, for comparison, we take the average of the summed spectrum as the characteristic spectrum of each knot in 3C 273 jet. Then, through the ratio of the observed to average flux densities of each knot and the aforementioned formula in § 2, we could derive a distribution of the Doppler factor in the spatially stratified emission regions of the 3C273 knots (Fig. 2). The error bars of derived Doppler factors could be evaluated from the ones of observed flux and the characteristic Doppler factor, and are also plotted in Fig. 2. Furthermore, by assuming a constant bulk velocity of the emission layers along the jet (we chose the bulk velocity that satisfies the average apparent velocity  $8c$  and the characteristic Doppler factor 7.4), we can obtain their equivalent viewing angle distribution of  $5^\circ$  to  $11^\circ$  with an average of  $7.7^\circ$  from their Doppler factor distribution. The averaged viewing angle distribution of emission layers in each knot could be explained by the combination of different equivalent viewing angle phases (i.e., near and away from viewing line) of different emission layers in each knot. As expected, the trend of the Doppler factor distribution is almost opposite to the equivalent viewing angle distribution.

The derived Doppler factors at radio frequency ( $\sim 10^{10}$  Hz) in each knot are almost the same (Fig. 2). This indicated that these radio-emitting electron regions are not independent. The Doppler factors at optical emission around  $10^{14}$  Hz in 3C273 knots are distinctly different from each other (Fig. 2), implying that these optical-emitting electron layers are likely to be independent. As these optical data are up to the break frequency of 3C273 knots, and the cooling effect of optical-emitting electrons is more severe than radio-emitting electrons, then the stratified effect of these optical-emitting electrons are also more obvious than radio-emitting electrons.

Based on our fits, the observed spectral shape of X-ray spectrum ( $\sim 10^{18}$  Hz) in the high-energy component actually reflects the spectrum of particles that emit photons at a frequency below  $5.51 \times 10^7$  Hz. Although the low-frequency emissions may be absorbed severely, the particles in the emission regions still could scatter off the CMB photons to the X-ray band. So, the Doppler factors of high-energy component actually represent the ones of low-energy component. Based on our modified stratified jet model as described in § 2, these below  $5.51 \times 10^7$  Hz radio-emitting electron regions mainly located nearer the jet surface, and are almost independent of those  $\sim 10^{10}$ Hz radio-emitting electron regions. Therefore, the Doppler factors of these two bands are also different. For the inner knots (such as knots A, B1, B2 and B3 in Fig. 2), the equivalent Doppler factors of the emission regions where the particles scatter the CMB photons to the X-ray band are larger than the ones of the emission regions that mainly emit photons between  $10^{10}$  and  $10^{15}$  Hz (see Fig. 2). This explains that the observed SEDs of the inner knots are dominated by the high-energy component (see fig. 2 of J07 and fig. 5 of U06). For the outer knots (such as knots D2H3, H2 and H1 in Fig. 2), the Doppler factors of the emission regions where the particles scatter the CMB photons to the X-ray band are overall smaller than the ones of emission regions that mainly emit photons between  $10^{10}$  and  $10^{15}$  Hz. This results in the observed SEDs of the outer knots to be dominated by the low-energy component. The intermediate knots (such as knots C1, C2 and D1 in Fig. 2) show almost identical Doppler factors among all the observed emission regions.

#### 4 CONCLUSION

Based on the hypothesis of the same intrinsic SED for all the knots in 3C 273 jet, the difference in their spectral shape is interpreted as a result of the difference of the equivalent Doppler factors of our modified stratified emission layers. Further, if we assume a constant bulk velocity of the emission regions along the

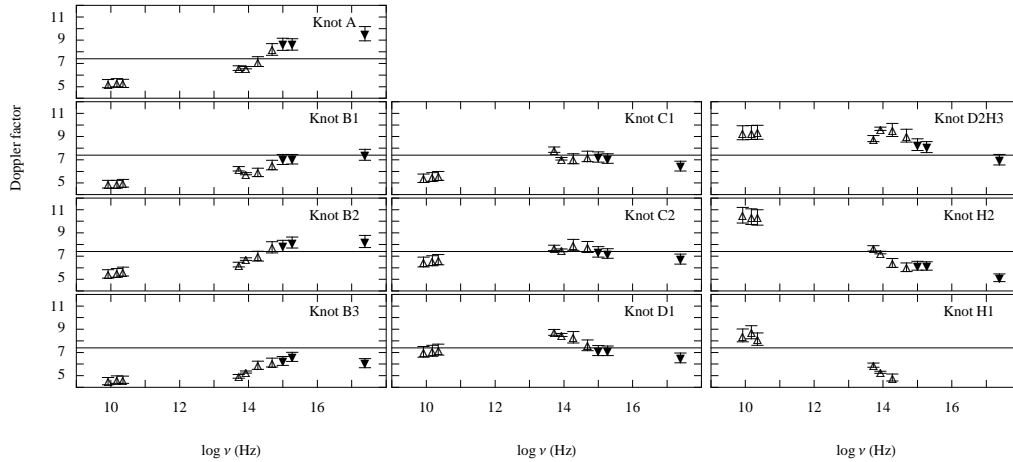


**Fig. 2** Distribution of the Doppler factor of each knot as a function of the observing frequency. The low-frequency component from radio to optical is plotted as empty-up-triangles, the high-frequency component as filled-down-triangles. The error bars are also plotted in the data. The left, middle and right panels show inner, intermediate and outer knots in 3C 273 jet respectively, with a characteristic Doppler factor of 7.4 in 3C 273 jet indicated by a straight line.

jet, the Doppler factor distribution could be due to the equivalent/averaged viewing angle distribution for the spatially stratified emission layers of the knots in 3C 273 jet. Our fitting to the summed spectrum supports that high energy  $X$ -ray emission is dominated by inverse Compton scattering of the cosmic microwave background. The predicted  $\gamma$ -ray spectrum of the large-scale jet in 3C 273 could be further tested by measuring its GeV spectrum from *GLAST* observations. It should be noted that our model needs the stratified synchrotron-emitting electrons, which should be verified by further multi-bands observations.

We thank S. Jester for helpful communications and supplying his data to us for reference. Many thanks are due to the referee for constructive comments.

This work has been partially supported by the National Natural Science Foundation of China (grants 10573029, 10625314, 10633010 and 10821302) and the Knowledge Innovation Program of the Chinese Academy of Sciences (Grant No. KJCX2-YW-T03), and sponsored by the Program of Shanghai Subject Chief Scientist (06XD14024) and the National Key Basic Research Development Program of China (No. 2007CB815405).

## References

- Aharonian, F. et al. 2002, *MNRAS*, 332, 215  
 Aharonian, F. et al. 2005, *A&A*, 441, 465  
 Bai, J. M. & Lee, M. G. 2003, *ApJ*, 585, L113  
 Blumenthal, G. R., & Gould, R. J. 1970, *Rev. Mod. Phys.*, 42, 237  
 Cao, X., & Bai, J. M. 2008, *ApJ*, 673, L131  
 Conway, R. G., Garrington, S. T., Perley, R. A., & Biretta, J. A. 1993, *A&A*, 267, 347  
 Dermer, C. D. 1995, *ApJ*, 446, L63  
 Flatters, C., & Conway, R. G. 1985, *Nature*, 314, 425  
 Georganopoulos, M., Perlman, E. S., Kazanas, D., & McEnery, J. 2006, *ApJ*, 653, L5 (G06)  
*GLAST* website, <http://fermi.gsfc.nasa.gov/>  
 Harris, D. E., & Krawczynski, H. 2006, *ARA&A*, 44, 463



- Jester, S., Harris, D. E., Marshall, H. L., & Meisenheimer, K. 2006, ApJ, 648, 900 (J06)
- Jester, S., Röser, H.-J., Meisenheimer, K., & Perley, R. A. 2005, A&A, 431, 477
- Jester, S., Röser, H.-J., Meisenheimer, K., Perley, R. A., & Conway, R. G. 2001, A&A, 373, 447
- Jester, S. et al. 2007, MNRAS, 380, 828 (J07)
- Kardashev, N. S. 1962, Soviet Astron., 6, 317
- Liu, L., 2006, ChJAA, 6, 663
- Lin, R.-G., 2001, ChJAA, 1, 245
- Liu, W.-P. & Shen, Z.-Q. 2007, ApJ, 668, L23 (LS07)
- Marshall, H. L., et al. 2001, ApJ, 549, L167
- Marshall, H. L., et al. 2002, ApJ, 564, 683
- Perlman, E. S., Biretta, J. A., Zhou, F., Sparks, W. B., & Macchetto, F. D. 1999, AJ, 117, 2185
- Perlman, E. S., & Wilson, A. S. 2005, ApJ, 627, 140
- Qian, S.-J., Zhang, X.-Z., Krichbaum, T.-P., et al. 2001, ChJAA, 1, 236
- Röser, H.-J., Meisenheimer, K., Neumann, M., Conway, R. G., & Perley, R. A. 2000, A&A, 360, 99
- Sambruna, R. M. et al. 2001, ApJ, 549, L161 (S01)
- Schimidt, M. 1963, Nature, 197, 1040
- Sreekumar, P. et al. 1994, ApJ, 426, 105
- Uchiyama, Y. et al. 2006, ApJ, 648, 910 (U06)
- Unwin, S. C. et al. 1985, ApJ, 289, 109
- Urry, C. M. 2006, <http://www.physorg.com/news70016047.html>
- Urry, C. M. & Padovani, P., 1995, PASP, 107, 803
- Wen, S.-L., Peng, Z.-M., Fan, J.-H., & Xie, G.-Z., 2002, ChA&A, 26, 398